Using a Plate FRF set to Identify a Damaged Site Without Employing a Reference Dataset

Horacio Valadares Duarte[1], Lázaro Valentim Donadon[1]

[1]*Dept. de Engenharia Mecânica da Escola de Engenharia da Universidade Federal de Minas Gerais*
Av. Antônio Carlos 6627, CEP 31270-901, Belo Horizonte, Minas Gerais, Brasil
hvduarte@ufmg.br, lazaro@demec.ufmg.br

Abstract. The procedure is based on the Energy Correlation Distance between each FRF (Frequency Response Function) collected on a grid and the set composed by all FRFs from a measurement mesh. To enhance the difference between a healthy and a damaged sites the FRF frequency sequence for highest modes is employed. This Energy Correlation Distance, at each grid point, is then treated using classical spacial statistical procedure, Krige method and Spatial Autocorrelation. To illustrate the procedure some initial results are included. Results for experimental data from composite plates and from a aluminium shell plate are presented. Remarks about the presented method improvements, limitations and restrictions are also incorporated.

Keywords: Energy Correlation Distance, Structural Health Monitoring, Frequency-based Damage Detection Method, spatial statistics, kriging

1 Introduction

The objective of this work is to determine a damage site using a FRF (Frequency Response Function) plate grid dataset. Complying with this, it is necessary to identify and quantify the differences between FRFs at different grid points. This space time analysis using a FRF is a challenging task because the FRF is not a single data it is a multivariable measurement (in a single spatial point there are a sequence of frequencies and associated amplitudes). The idea is to use a procedure or a function that using two FRFs returns a unique value, if this function satisfy the metric axiom (separation condition, symmetry and triangle inequality), a proper use of this metric distance could accomplish the outlined objective.

A recent proposed procedure is the Energy Covariance and Correlation Distance introduced by Székely, Rizzo and Bakirov [1]. Energy Distance is a distance between probability distributions (Rizzo[2]). It applies to random vectors in arbitrary dimensions, and the methodology requires only the mild assumption of finite first moments (Rizzo [2]). There are many routines for different areas as reported by Rizzo [2] mainly, but not only, in times series analysis where identify temporal dependence structure on time series is an important issue (Zhou [3], Pitsillou [4]).

For this work, beyond simplicity, the main aspect of the Energy Correlation Distance is the property of the coefficient $\mathcal{R}_n^2(X,Y)$. For variables X and Y with finite first moments (finite mean), all possibilities for $\mathcal{R}_n^2(X,Y)$ lies on the range $0 \leq \mathcal{R}_n^2(X,Y) \leq 1$. $\mathcal{R}_n^2(X,Y) = 0$ only if X and Y are linearly independent and $\mathcal{R}_n^2(X,Y) = 1$ only if there is a linear dependence between X and Y. This is important because $\mathcal{R}_n^2(X,Y) = 0$ does not hold for linear independent sets for general metric spaces , only for separable ones (Lyons [5]). The Energy Distance $\mathcal{R}_n^2(X,Y)$ satisfies all axioms of a metric distance, (Székely [1]), that are valid not only for Euclidean metric although it is used in following revision. The authors also highlights that Distance correlation can be applied as an index of dependence, (Székely [1]), more important, without requiring distributional assumptions (Székely [6]).

A problem with $\mathcal{R}_n^2(X,Y)$ statistic is the bias increasing with sample dimension. Szekely and Rizzo [7] introduced the unbiased distance correlation $\mathcal{R}_n^*(X,Y)$ to overcome this drawback. The remarkable difference is that $\mathcal{R}_n^*(X,Y)$ lays in interval $-1 \leq \mathcal{R}_n^*(X,Y) \leq 1$, but $|\mathcal{R}_n^*(X,Y)| \leq 1$ satisfy the triangle

inequality inheriting all other properties of the $\mathcal{R}_n^2(X,Y)$ statistic[7].

Defined $\mathcal{R}_n^*(X,Y)$ as the metric distance between FRFs, the next step is to implement a procedure that can use this metric properties efficiently exploring the structural characteristics. The main idea came from a statement of the spatial statistic that near points have close properties [8], so nearest points should present similar FRFs or FRF distances close to 1. The FRF unbiased correlation distances between two nearest points is an important information about local structural health.

In this work a procedure similar to many mode extraction technique will be used, the FRF will be analysed using FRF frequency range in a vicinity of a frequency mode. This procedure is employed because there is a expected displacement change in the neighbourhood of the damaged site. In the Fig. 1 a graphical interpretation of this phenomena that will be more significant for high frequency modes. In the reference Duarte and Donadon[9] a more detailed discussion about this behaviour.

The identification procedure is based on the following steps and assumptions:

1- stablish a metric distance to quantify the distances between two FRFs;

a - from spatial statistics the nearest points presents similar properties[8];

b - although not strictly necessary, a reference will be employed. The reference is the complete FRF dataset. So the distances will be computed between FRFs from a single point to the complete FRF dataset including the FRF whose distance to the set is been computing.

2- the FRFs distances will be analysed in similar fashion of many mode extraction procedures. There will be an analysis in the vicinity of each natural frequency and not using the entire FRF frequency.

a - the wavelength of the mode shape,λ, reduces with frequency increase, Fig. 1, and there is a strain

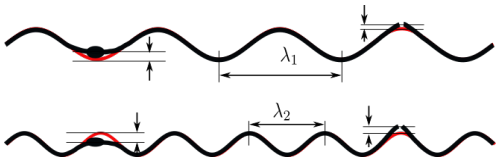

Figure 1. Strain energy rising with frequency increases the difference between damaged and healthy areas.

energy enhancement highlighting the damaged sites [9].

3- the result of applying all previous steps is the distance to the reference, a scalar data, at the grid nodal points for each natural frequency.

4- In this work the kriging method is employed to analyse this scalar spatial data. This procedure allows to identify discrepancies by modelling deterministic data trend and the stochastic component independently.

5- kriging method is a linear interpolation method and will be employed to check the spatial discrepancies using the expected symmetry of the dynamical response of the symmetrical structures.

The reported results in this work are from symmetrical structures and this procedure will ensure a more smooth distances between closest and symmetric points. The objective is to enhance symmetry from interpolation procedure as this could help to exhibit an odd measurement.

2 The Energy Distances

As stated the algorithm Coefficient for Covariance Correlation Distances are very simple. From classical Euclidean distance matrix a_{ij} defined as $a_{ij} = |x_i - x_j| = \left[\sum_{k=1}^{p}(x_{ik} - x_{jk})^2\right]^{\frac{1}{2}}$, where $x_k \in \mathbb{R}^p$, $x_k \subset X^{n,p}$. Similarly $y_l \subset Y^{n,q}$ defines a Euclidean distance matrix $b_{ij} = |y_i - y_j|$. The bi-centered matrix A_{ij} is computed from Euclidean matrix, $A_{ij} = a_{ij} - \bar{a}_i - \bar{a}_j - \bar{a}$, where

$$\bar{a}_i = \bar{a}_{i,} = \frac{1}{n}\sum_{k=1}^{n} a_{i,k} \qquad \bar{a}_j = \bar{a}_{,j} = \frac{1}{n}\sum_{k=1}^{n} a_{k,j} \qquad \bar{a} = \frac{1}{n^2}\sum_{i,j=1}^{n} a_{i,j} \tag{1}$$

B_{ij} is computed using similar procedure $B_{ij} = b_{ij} - \bar{b}_i - \bar{b}_j - \bar{b}$.

The Székely paper [7] work starts with the observation that the bias of the $\mathcal{R}_n^2(X,Y)$ statistic increases with dimension. For $X_{n,p}$ and $Y_{n,q}$ when $p,q \to \infty$ then $\mathcal{R}_n(X,Y) \to 1$ and $\mathcal{V}_n(X,Y) \to \infty$. Székely [7] propose the bias corrected $A_{i,j}^*$ and $B_{i,j}^*$ matrices using the previous defined matrices $a_{i,j}$, $b_{i,j}$, $A_{i,j}$ and $B_{i,j}$

$$A_{i,j}^* \begin{cases} = \dfrac{n}{n-1}\left(A_{i,j} - \dfrac{a_{i,j}}{n}\right), & i \neq j \\ = \dfrac{n}{n-1}\left(\bar{a}_i - \bar{a}\right), & i = j \end{cases} \quad \text{and} \quad B_{i,j}^* \begin{cases} = \dfrac{n}{n-1}\left(B_{i,j} - \dfrac{b_{i,j}}{n}\right), & i \neq j \\ = \dfrac{n}{n-1}\left(\bar{b}_i - \bar{b}\right), & i = j \end{cases} \tag{2}$$

The Unbiased Distance Covariance statistics $\mathcal{V}_n^*(X,Y)$ and Unbiased Distance Correlation coefficient $\mathcal{R}_n^*(X,Y)$ are

$$\mathcal{V}_n^*(X,Y) = \frac{1}{n(n-3)}\left[\sum_{i,j=1}^{n} A_{i,j}^* B_{i,j}^* - \frac{n}{n-2}\sum_{i=1}^{n} A_{i,i}^* B_{i,i}^*\right] \quad \text{and} \quad \mathcal{R}_n^*(X,Y) = \frac{\mathcal{V}_n^*(X,Y)}{\sqrt{\mathcal{V}_n^*(X,X)\mathcal{V}_n^*(Y,Y)}} \tag{3}$$

if the Distance Covariances $\mathcal{V}_n^*(X,X) = 0$ or $\mathcal{V}_n^*(Y,Y) = 0$ then $\mathcal{R}_n^*(X,Y) = 0$. Also the empirical statistical coefficients $\mathcal{V}_n^*(X,Y)$ and $\mathcal{R}_n^*(X,Y)$ converge almost surely to the population coefficients $\mathcal{V}^*(X,Y)$ and $\mathcal{R}^*(X,Y)$ as $n \to \infty$. As stated the $-1 \leq \mathcal{R}_n^*(X,Y) \leq 1$, but $0 \leq |\mathcal{R}_n^*(X,Y)| \leq 1$ and satisfy the triangle inequality and the metric axiom[7].

3 Kriging Spatial Interpolation

The Correlation distances $\mathcal{R}_n^*$ obtained at each grid point of the plate are analysed using the kriging interpolation method. As there are few data points the interpolation will allow a better interpretation of the results to check the spatial discrepancies.

The kriging is a well known and tested spatial estimation procedure and it will not be extensively reviewed. In the reference van Lieshout [10] a short and well grounded introduction to spatial kriging, the extended concept to spatio temporal kriging the reference Wikle et al. [8] is a more appropriate reference, in the Pebesma [11] is a short review also showing a practical application of the method. The kriging method is a linear interpolation at position z_o based on a spatial model constructed from the known space point variable values, z.

$$Y^*(z_o) = \sum_{i}^{N} \lambda_i Y(z_o) + m(z_o) \tag{4}$$

where $z_o = (x_k, y_k)$ is the z_o coordinates and $Y^*(z_o)$ is the estimation at unobserved positions z_o using a weighted values λ_i computed from known positions z. The term $m(z)$, $m(z) = \beta_o + \beta_1 f_1(z) + \beta_2 f_2(z) + \ldots$ is the fitted deterministic term of the equation.

The procedure is based on the spatial stationarity, there are the assumption that the mean can be estimated by the arithmetic mean of a stochastic data. For a random, or Gaussian, distribution this term is a constant mean, $m(z_o) = \mu$, and the procedure is named simple kriging. It means that there is no tendency of the data values $Y(z)$ with position z. Ordinary kriging is applied when $m(z_o)$ is locally constant or can be considered locally constant. The universal kriging is used if there is a spatial trend or spatial data correlation, $m(z)$, that must be considered. The $\sum_i^N \lambda_i Y(z_o)$ term is intended to be applied to a random data, if there is a trend, then it should be applied on residual of the spatial correlation $m(z_o)$. The algorithm is distinct for each case.

The second stationarity principle can be stated as follow: the correlation between two random variables solely depends on the spatial distance between them, and does not depend on their location or position. If $|z_i - z_k| < h$ the correlation $C(z_i, z_k) = C(h)$

$$C(z_i, z_k) = \frac{1}{K}\sum (Y(z_i) - m(z_i))(Y(z_k) - m(z_k)) = \frac{1}{K}\sum (Y(z_i) - m(h))(Y(z_k) - m(h)) \tag{5}$$

$K = \sum k$ for $|z_i - z_k| < h$ and

$$m(h) = \frac{1}{2N}\sum \left(Y(z_i) + Y(z_k)\right) \tag{6}$$

Based on these principles the next step is to fit data or its residual to a tested family of variogram models (Spherical, Exponential, Linear etc) Pebesma [12, 13]. The objective is to select a model that minimizes the variance with distance, the stochastic spatial model, allowing to create a system of equations to determine λ_i. In the kriging method there is a deterministic term, $m(z)$, the interpolation term to handle the global data trend and a stochastic term, $\sum_i^N \lambda_i Y(z_o)$, considering the randomness in the data[10].

4 Data, Measurements and Analysis

The data employed to analyse the proposed method was not obtained from a experiment projected specifically to test this procedure. The first dataset is from a aluminium plate monitored by 36 PZT grid

sensors and second dataset is from a laminate plate monitored by a accelerometer attached in a unique single position. In both cases the system is excited by the a hammer. The data analysis was performed using the public packages from R Project for Statistical Computing `https://www.r-project.org/`. The distance correlation is computed using the package: *energy*, kriging method: $sp, gstat$[11], kriging variogram optimization: *automap*, and graphical: $raster, ggplot2$.

4.1 The Aluminium Plate

The first structure is a square aluminium plate, 1 m×1 m, thickness×1.0×10^{-3} m and 2.7 kg, data from vendor. It was hanged up by two symmetrical thin nylon wire, Fig.2. The measurement grid is composed by a squared mesh, each side with $18{\times}10^{-3}$ m (180 mm) length. The passive or measurement PZT sensor is attached at the grid points by a thin bond epoxy layer. The PZT sensor has an effective diameter $D_{PZT} \approx 6.5$ mm, with an area of $3.318{\times}10^{-5}$m^2 and are from Acellent Technologies.

Experimental data acquisition was performed by the PHOTON II from LDS. Measurements were done using a excitation hammer, the original FRFs have units mV/Newton (response/excitation or X_i/F_j) from 0 to 560 Hz using a sampling rate of 1280 Hz. The hammer is a PCB model 086C05, the signal used in this work employs only response to excitation at the same position or X_i/F_j only for $i = j$. The excitation was done using the hammer on the plate face just behind the sensor position.

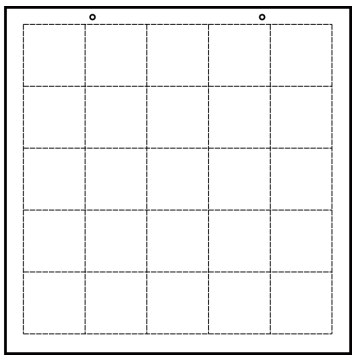

Figure 2. Aluminium plate, PZT sensor measurement grid layout

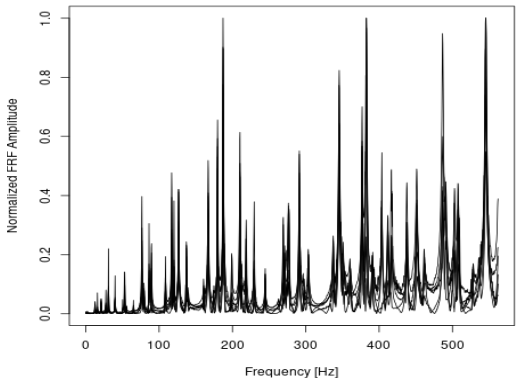

Figure 3. FRFs from Aluminium plate

Data Analysis from Aluminium Plate

There are no damage inside the grid measurement area, the procedure is employed to check some assumptions in the proposed procedure and to check some measurement aspects and experimental results that could bother the analysis.

In the FRFs frequency range, from 0 to 560 Hz, Fig. 3, were identified 54 natural frequencies. Each FRF was normalized using weighted values by setting the FRF maximum to 1, avoiding strong amplitude discrepancies between FRFs. As stated, the frequency range in the vicinity of each natural frequency is analysed, the distances computed at grid points and a ordinary kriging is performed for this frequency. In figure 4 some results using ordinary kriging interpolation.

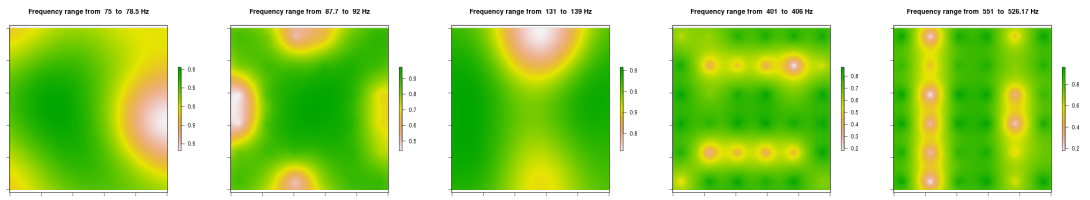

Figure 4. Kriging interpolation graphics.

The main assumption to be checked is the symmetry because there is no damage and the structure is symmetric. The majority of the interpolation panels presented some kind of symmetry but this symmetry is not perfect. Analysing the symmetry was defined the V_c vertical and H_c horizontal coordinates of the

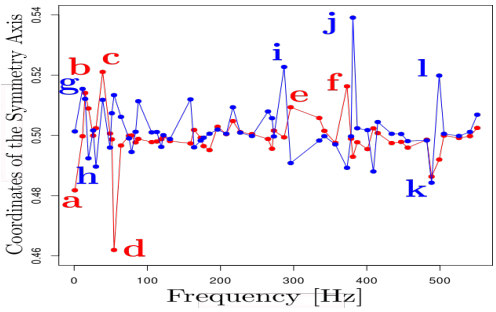

Figure 5. Coordinates of the symmetry axis, vertical, V_c, in blue lines, and horizontal, H_c, in red lines

symmetry axis of the kriging interpolated panels.

$$V_c = \frac{\sum x_i \mathcal{R}_i^*}{\sum \mathcal{R}_i^*} \qquad and \qquad H_c = \frac{\sum y_i \mathcal{R}_i^*}{\sum \mathcal{R}_i^*} \tag{7}$$

Figure 5 shows the variations of the symmetry axis with frequency, the vertical axis, V_c, is plotted in blue lines, red lines for the horizontal, H_c. The plate center coordinates are x_c=0.5 m and y_c=0.5 m. Using this Fig. 5 the most significant axis displacement were selected and the correspondent kriging panels are plotted. In Fig. 6 there are panels for significant displacement axis H_c labelled by original letter case. For the symmetry axix V_c, the equivalent panels are plotted in Fig. 7. In Fig.6, panel **d**, and in

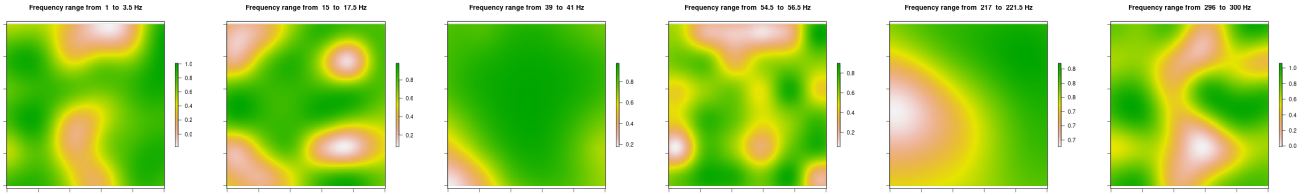

Figure 6. Kriging interpolation graphics for great displacement of the horizontal symmetry axis.

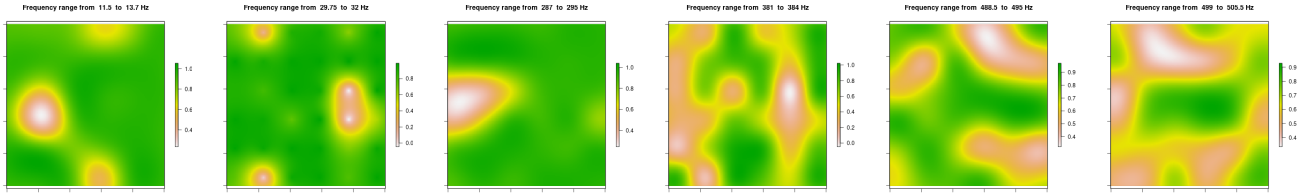

Figure 7. Kriging interpolation graphics for great displacement of the vertical symmetry axis.

Fig.7, panels **j**, **k** and **l**, these panels are from a close neighbourhood sequence of modes or twin mode cases. This means that there is no clear separation between the modes, the panels from them are not well defined, but, by chance, one of them can presents a big asymmetry captured by axis displacement. For highest frequencies the panels are less defined too, the size of the grid mesh and the reduction of the hammer energy with frequency could explain this behaviour. The panels in Fig. 6-**a** and **d** seems to be related to the suspension area of the plate.

4.2 The Composite Plate

The composite data is from a nanocomposite laminate plate and was used in a modal analysis to determine its mechanical properties, Duarte et al. [14]. The S2-glass/epoxy-nanoclay composite is a laminate plate with 16 layers and a 65% fiber volume fraction. The nanoclay particles used are organically modified montmorillonite in a platelet form, while the S2-glass fiber has a plain-weave woven fabric configuration with a density of 180 g/m2 from Texiglass. The total mass of the plate is 6.527×10^{-2} kg (65.27 grams).

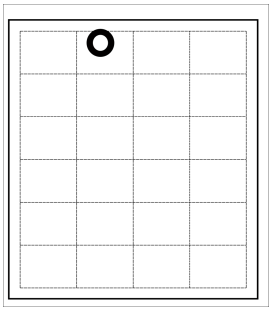

Figure 8. Composite plate measurement layout

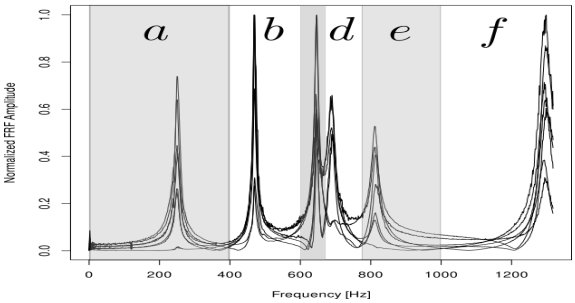

Figure 9. FRFs from composite plate

The FRF measurement was taken in a rectangular plate with dimensions $1.36{\times}10^{-1}$ m (136 mm) × $1.16{\times}10^{-1}$ m (116 mm) × $2.4{\times}10^{-3}$ m (2.4 mm). There are 35 grid points, 5 × 7 divisions per side.

The excitation is performed by a hammer PCB 086C05. The hammer excites at each grid point while the accelerometer remains in the same position in all measurements. Experimental data acquisition was performed by the PHOTON II, the FRFs have units g/Newton in a frequency range from 0 to 1300 Hz using 3000 Hz sampling rate, the normalized FRFs are in Fig.9. The acceleration transducer is a PCB miniature, type 352A71, with a mass of $6.40{\times}10^{-4}$ kg (0.64 grams) at about 1.0% of the plate mass.

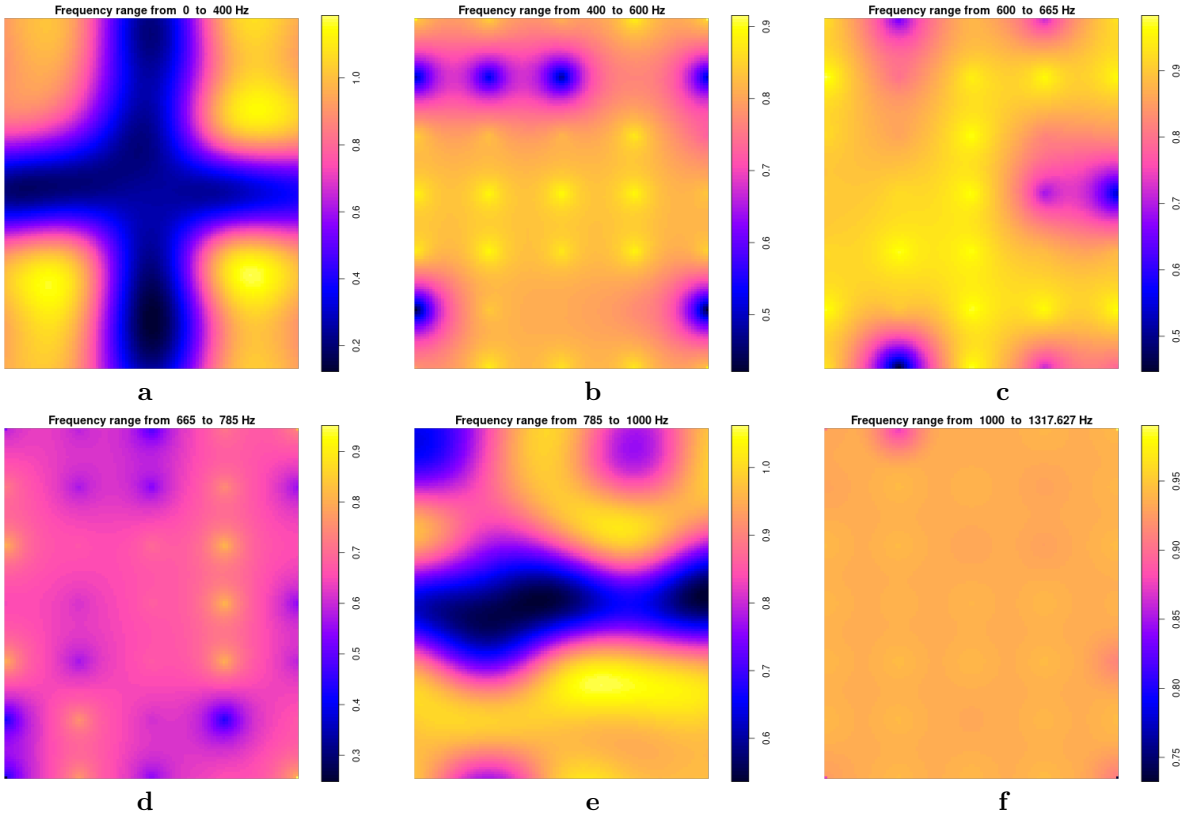

Figure 10. Kriging interpolation graphics for laminate plate.

The objective of this section is to check the capability of the method to identify the position of the accelerometer. Of course it is not a real damage but the accelerometer attached to the plate surface promotes a perturbation in the structure response. The 1% mass ratio between accelerometer and the plate mass can be considered a good test. The accelerometer position is the circular mark in Fig. 8.

Composite Plate Data Analysis

In Fig. 10 the panels from applying the kriging method to the grid point correlation distance, $\mathcal{R}^*_{i,j}$. The panels are labelled with the frequency range identification showed in Fig.9. The panels were obtained from flagged frequency range. There is not a perfect symmetry also. There is a horizontal and vertical symmetry in the panel Fig. 10-**a**, a horizontal symmetry can be viewed in panels **c** and **e**, and a vertical

symmetry in the panel Fig. 10-**b**. There is no symmetry in the graphics **d** and **f**. The panels in Fig. 10-**c** and Fig. 10-**d** are from a twin mode frequency range, and the panel **d** is the most ill-defined graph.

The Fig. 10-**f** is very different from the previous ones. There are faint areas protruding from an almost similar measuring level, the biggest and more intense anomaly is closest to the accelerometer position. There is no more modes to assert that it is an indication of the sensor position, but all characteristics of the graph points to this direction and the sensor is not positioned in grid point.

5 Conclusions

The proposed method for damage site identification based on distance correlation metrics and kriging spatial interpolation presents promising results. With few improvements this is a simple method to analyse locally symmetrical or mirrored parts. Structures are usually symmetrical, using this property is not necessary to analyse the full structure to monitory it.

Authorship statement. The authors hereby confirm that they are the sole liable persons responsible for the authorship of this work, and that all material that has been herein included as part of the present paper is either the property (and authorship) of the authors, or has the permission of the owners to be included here.

References

[1] G. J. Székely, M. L. Rizzo, and N. K. Bakirov. Measuring and testing independence by correlation of distances. *The Annals of Statistics*, vol. 35, n. 6, pp. 2769–2794, 2007.
[2] M. L. Rizzo and G. J. Székely. Energy distance. *WIREs Computational Statistics*, vol. 8, pp. 27–38, 2016.
[3] Z. Zhou. Measuring nonlinear dependence in time-series, a distance correlation approach. *Journal of Time Series Analysis*, vol. 33, n. 3, pp. 438–457, 2012.
[4] D. Edelmann, K. Fokianos, and M. Pitsillou. An updated literature review of distance correlation and its applications to time series. *International Statistical Review*, vol. 87, n. 2, pp. 237–262, 2019.
[5] R. Lyons. Distance covariance in metric spaces. *Ann. Probab.*, vol. 41(5), pp. 3284–3305, 2013.
[6] G. J. Székely and M. L. Rizzo. Brownian distance covariance. *The Annals of Applied Statistics*, vol. 3, n. 4, pp. 1236–1265, 2009.
[7] G. J. Székely and M. L. Rizzo. The distance correlation t-test of independence in high dimension. *Journal of Multivariate Analysis*, vol. 117, pp. 193–213, 2013.
[8] C. K. Wikle, A. Zammit-Mangion, and N. Cressie. *Spatio-Temporal Statistics with R*. Chapman & Hall/CRC, Boca Raton, Florida, 2019.
[9] H. V. Duarte and L. V. Donadon. Frequency-based damage detection method for excitation signals above work frequencies: theoretical aspects and experimental results. *Journal of the Brazilian Society of Mechanical Sciences and Engineering*, vol. 43, n. 1, 2021.
[10] van M. Lieshout. *Theory of Spatial Statistics A Concise Introduction*. Chapman & Hall/CRC, Boca Raton, Florida, 2019.
[11] E. J. Pebesma. The role of external variables and gis databases in geostatistical analysis. *Transactions in GIS*, vol. 10, n. 4, pp. 615–632, 2006.
[12] E. J. Pebesma. Multivariable geostatistics in S: the gstat package. *Computers & Geosciences*, vol. 30, pp. 683–691, 2004.
[13] E. Pebesma and B. Graeler. Spatial and spatio-temporal geostatistical modelling, predictionand simulation, r package gstat version 2.0-7. `https://github.com/r-spatial/gstat`, 2021.
[14] H. V. Duarte, L. V. Donadon, and A. F. Ávila. Mechanical properties of nanocomposite laminated structure and its sensibility to modal analysis procedure. *Latin American Journal of Solids and Structures*, vol. 11, n. 2, pp. 245–259, 2014.